Sedimentation in colloidal gels

by

Hessah Alharbi

B.S., Qassim University, 2014

A THESIS

submitted in partial fulfillment of the requirements for the degree

MASTER OF SCIENCE

Department of Physics
College of Arts and Sciences

KANSAS STATE UNIVERSITY
Manhattan, Kansas

2021

Approved by:

Major Professor
Christopher Sorensen

Copyright

Abstract

This study investigates the effect of stability ratio (W) on the sedimentation of colloidal gels. We monitored the temporal evolution of the gel height within our experimental time that lasted between 7-10 days. We found that some gels sediment while others do not. For sedimenting gels, the sedimentation height reaches an asymptotic value (H_a). In addition, we found that the temporal evolution of the sedimentation height profile depends on W in two manners. First, the characteristic time of the sedimentation height, t_c, increases with decreasing W. In other words, the higher the W, the faster the sedimentation process. Second, we found that H_a decreases with increasing W.

Table of Contents

List of Figures

List of Tables

Acknowledgments

First, I would like to express my deepest gratitude to my advisor Dr. Chris Sorensen for his continuous support during my Master's thesis. His patient encouragement and valuable advice have guided me during this work. Thank you, Dr. Sorensen, for giving me the opportunity to join your group and work with you.

Second, I would also like to thank Dr. Loren Greenman and Dr. Daniel Rolles, for being my committee members.

Finally, I would like to thank Raiya Ebini for guiding me during the lab experiments. Also, her constructive suggestions have helped me to improve my thesis. For that, I am grateful.

Dedication

Dedicated to my family

1 Colloidal Gelation and Sedimentation

A colloid has two immiscible phases. It contains particles of one substance dispersed throughout a second phase, the suspending medium. The dimension of the dispersed phase can range from a few nanometers to a few micrometers. The colloids can be classified into various groups depending on the nature of the dispersed substance and the suspending medium, such as suspension, emulsion, or soot. Colloids are ubiquitous in the food, drug, cosmetic, and oil industries.

Colloidal systems can form fractal aggregates. One can starts aggregation in any colloidal system by destabilizing them. There are different methods of destabilizing a colloidal suspension. For example, changing the pH of the solution, adding salt or polymers to the solution. For a high enough particle volume fraction and destabilization attraction within the solution, the colloids not just aggregate but may have the chance to form a space-filling network, a gel. The gel might experience sedimentation under gravity due to the mismatch between the particle density and the dispersed solvent (Condre et al., 2007).

In this work, we used $MgCl_2$ to destabilize the colloidal particles. This will create an interaction known as Derjaguin-Landau-Verwey-Overbeek (DLVO). In this chapter, I will discuss the (DLVO) since it is the primary interaction that controlled the gel sample I prepared in the lab.

1.1 Fractals Aggregates

Fractals are objects with invariant scales (Mandelbrot,1977). This means the object looks the same regardless of its different size. The same geometry can be seen with zooming in or zooming out. Fractals are often looked self-similar. This implies that any part of the object represents the whole structure. Generally, the number of replicates of a linear size can be used for describing a self-similar fractal. Thus, the mass of fractal objects scale with their linear size as follows:

$$mass \sim (linear\ size)^{D_f} \tag{1.1}$$

Where D_f is the scaling dimension known as fractal dimension. D_f distinguishes the morphology of one fractal object from another, and it is smaller than the spatial dimension, d. Figure 1.1 shows an example of a fractal geometry and its fractal dimension. Regardless of the number of iterations, the geometry would have $D_f = 1.58$.

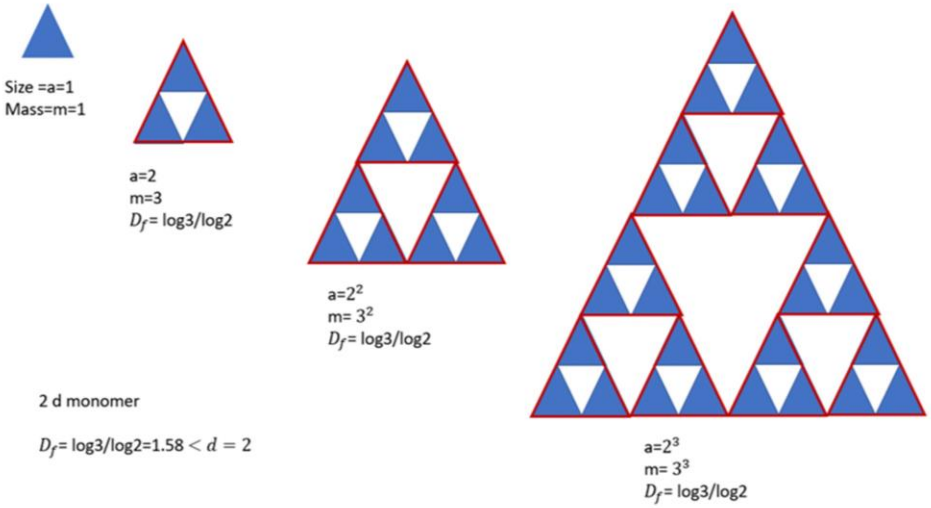

Figure 1.1. Two dimensional particles joining together to create fractals with $D_f < d$.

1.2 DLVO Interaction

When colloidal particles destabilized, they start to form aggregates. In charge-stabilized colloids, the destabilization can be induced by adding salt to the solution. This will create the DLVO potential. The DLVO theory of colloidal dispersion describes how the ionic surfaces of two particles overlap, and a repulsion force evolves as they approach each other. By adding salt, the solution ionic strength changes and screens the electrostatic repulsion, enabling the particles to come together and stick. In this theory, colloidal stability is affected by two forces: the attractive van der Waals forces and the repulsive electrical double layer forces. DLVO interaction can be written as a sum of the electrostatic repulsion, U_R, and the van der Waals attraction, U_A (Derjaguin and Landau 1941; Verwey, Overbeek, and Van Nes 1948).

$$U_{DLVO} = U_R + U_A \tag{1.2}$$

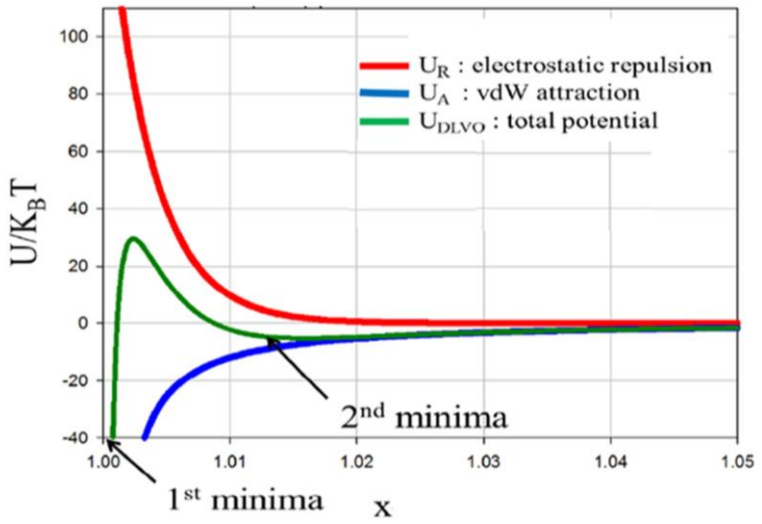

Figure 1.2. DLVO interaction (Ebini, 2020).

1.3 Gel Formation

Colloidal gels can be produced by inducing the interaction between colloidal particles. When non-coalescing colloidal particles are under the influence of an attractive potential, they tend to form fractal aggregates. If initial particle and salt concentrations permit, these fractal aggregates will continue to grow until there is no remaining open, non-aggregating space in the system. Hence it forms a fractal gel.

The mass of fractal aggregates can be represented by the number of monomers in an aggregate, N. Because these are fractals, then N, scales with its radius of gyration, R_g, as

$$\mathrm{N} = k_0 \left(\frac{R_g}{\mathrm{a}}\right)^{\mathrm{D_f}} \tag{1.3}$$

Where a is the radius of the monomers, k_0 is the prefactor of order unity. From equation 1.3, we can write $R_g \sim N^{1/D_f}$. The average nearest neighbor separation R_{nn} is related to the total number of clusters N_c in a system of volume V by

$$\mathrm{R_{nn}} \sim \left(\frac{\mathrm{N_c}}{\mathrm{V}}\right)^{-\left(\frac{1}{\mathrm{d}}\right)} \tag{1.4}$$

Assuming all clusters in a system have the same size, the number of clusters is proportional to the total number of monomers in the system, N_m. So, one can write $N_c = N_m / N$, which yields $R_{nn} \sim N^{1/d}$.

The transformation of a system of small particles, sols, to aggregates, and then to a gel is known as the sol-to-gel transformation .The main length scales R_g and R_{nn} can define the kinetics of this transformation. Based on those length scales, the Ideal Gel Point theory (IGP) specifies three distinct aggregations. First, when the aggregates are very far apart, $R_{nn} \gg R_g$, the cluster-dilute regime will be identified. At $R_{nn}/R_g \lesssim 10$, the system will evolve from the cluster-dilute to the cluster-dense regime. Because $D_f < d$, R_g will grow faster than R_{nn} until they become comparable, then we can say the system gel at $R_{nn} \sim R_g$. Assuming all the clusters are spherical and have the same size. Therefore, the radius of gyration at the gel point. $R_{g,G}$ can be determined when the volume fraction of clusters is about one from (Ebini & Sorensen, 2019; Sorensen & Chakrabarti, 2011)

$$\mathrm{R_{g,G}} = \mathrm{a}\left[\mathrm{f_{vm}^{-1}\, k_0}\left(\frac{\mathrm{D_f}}{2+\mathrm{D_f}}\right)^{\frac{3}{2}}\right]^{1/(3-\mathrm{D_f})} \tag{1.5}$$

Where f_{vm} is the monomer volume fraction. Figure 1.3 shows a sketch of the evolution of R_g and R_{nn} in an aggregating sol versus the number of monomers per aggregate <N>.

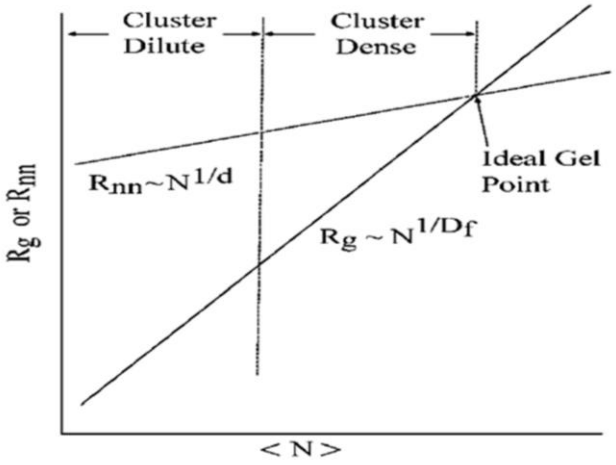

Figure 1.3. The sol-to-gel transformation (Sorensen & Chakrabarti, 2011).

For fractal aggregates, two limiting regimes of aggregation have been defined: diffusion limited cluster-cluster aggregation (DLCA); and reaction limited cluster-cluster aggregation (RLCA). The sticking probability, P, is the main difference between these two limiting regimes ,which can define the number of times the particles need to collide before they stick. This can be dominated by the strength of interaction that was induced to destabilize the particles and start the aggregation. For the (DLCA) system, any two particles that meet will immediately become irreversibly bound together with strong, short-range attraction. Aggregation in this system may occur very fast at sufficient volume fractions with no rearrangement of particles once they have met with sticking probability, P ~ 1. This yields a fractal dimension, D_f = 1.8 (Asnaghi et al., 1994; Lin et al., 1989a; Weitz et al., 1985). If, instead, the attraction is weak, in other words, P

<<1, the monomers will need to collide so many times before they stick together. This allows the monomers to penetrate deep in the aggregate and hence create a denser fractal. This is known as the RLCA regime with a $D_f = 2.15$. (Lin et al. 1989c; Weitz et al. 1985) and $D_f \sim 2.14$ (Lin et al. 1989c).

1.4 Gel Collapse

After a gel forms, it may experience sedimentation under gravity. A gel collapses with an interface in which separates the suspending medium from the colloidal gel. Several studies have been devoted to gel collapse using a variety of techniques and different kinds of colloidal gels. This involves changing volume fraction of colloidal particles (Allain et al., 1995; Harich et al., 2016), interaction strength (Harich et al., 2016; Starrs et al., 2002), particles size (Kim et al., 2013), and even varying gel samples height and width (Starrs et al., 2002).

Allain et al. studied a gel system of calcium carbonate particles(Allain et al., 1995). The size of the particles was 70nm in diameter, with a density of 2.7g/cm^3. The system was destabilized by adding salt to the solution. They studied the time evolution of the suspension as a function of the volume fraction, f_{vm} in the range ($1 \times 10^{-4} < f_{vm} < 3 \times 10^{-2}$). They observed three sedimentation behaviors. First, at low volume fractions, the clusters formed, but the system never gelled. Instead, the clusters settled independently and grew in the process. This was referred to as cluster deposition. Second, for higher volume fraction, the samples create a gel first and then sediment later under its own weight. A sharp interface separates the settling suspension from the clear supernatant. This interface moves downward until it reaches an equilibrium height. The latter category was referred to as collective settling. The third observation was for high enough volume fractions were sample gelled but never sediment.

Kim et al. used adhesive hard spheres to study gel collapse. They used particles of size 30, 100, and 300 nm with keeping the same interaction potential for different volume fractions. They found that the gravitational Peclet number, Pe of ~ 0.01 is the value that predicts gel stability for the particles they used. Where Pe is a function of particle size, volume fraction, and gravitational acceleration (Kim et al., 2013).

Harich et al. used depletion interaction to destabilize colloids of radius 326nm with a density mismatch of 0.253g/cm^3 (Harich et al., 2016). The study was done with varying the volume fraction, which ranges from 0.05-0.5, and polymer concentrations. To monitor the gel collapse, they used magnetic resonance imaging to provide quantitative, spatio-temporally resolved measurements of the solid volume fraction in the rapid collapse of gels. They recorded the gel interface height and plotted its time dependence as the scaled height H'(t)

$$H'(t) = \frac{(H(t) - H_a)}{(H_0 - H_a)} \tag{1.6}$$

Where H_o is the sample initial height and H_a is the sample final height of the sedimentation. Here H_a was taken as $h_{rcp} = 0.64$, which is the height of random-close-packed sediment. The gravitational collapse of the gels falls into two distinct regimes as a function of colloid and polymer concentrations. The first one is the delayed rapid gravitational collapse, as shown in figure 1.4 (a). The other one is a stretched exponential decay, as shown in figure 1.4 (b). For the first one, the gel starts with a delay time where gels are gravitationally stable. Then a rapid linear collapse occurs, followed by a slow stretched exponential, which stops at a well-defined sediment height. MRI imaging showed that a dense region forms at the top of the sample

during the delay time. As the gel structure can no longer support this dense layer, rapid collapse occurs. In the second regime, the system starts with longer delay times followed by a stretched exponential with no linear rapid collapse. The stretch exponential they obtained was found to be much smaller than the one found for smaller particles.

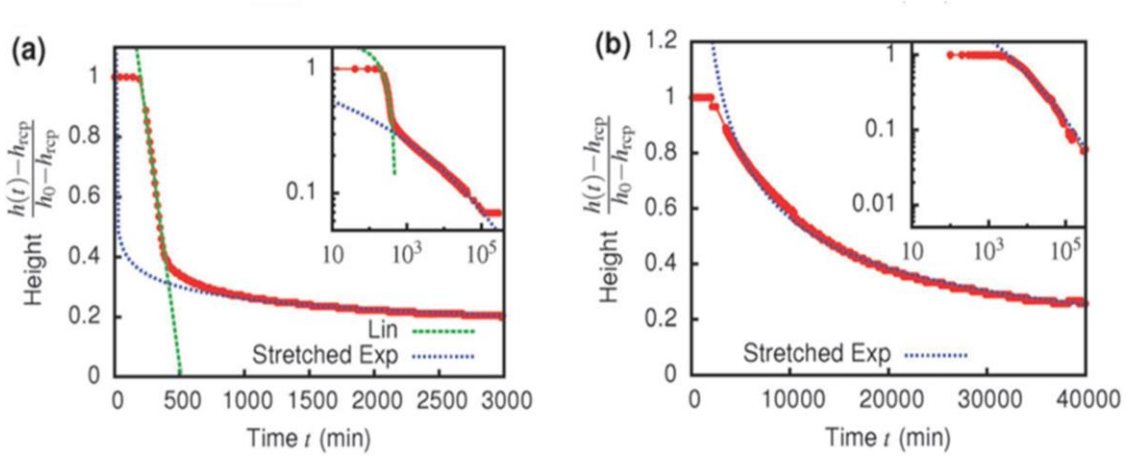

Figure 1.4. Normalized height H'(t) vs. t_w for samples that show (a) delayed sedimentation, (b) stretched exponential slow sedimentation (Harich et al., 2016).

Starrs et al. used depletion interaction to destabilize colloids with radius 186nm (Starrs et al., 2002). They study samples above the gel boundary. They found, similar to Harich et al., for relatively low polymer concentration, the samples go through delayed sedimentation followed by a rapid collapse. Whereas for high polymer concentration, they observed a stretched exponential sedimentation they call it creeping. For delayed sedimentation, they found the delay time increases with increasing the attraction strength and the container aspect ratio, height/width. At

the same time, they reported the creeping sedimentation to be a function of the cuvette size compared to the characteristic size of the gel.

For the delayed sedimentation, they observed two features: channeling and streamer formation. Both cause local breaking of the gel but do not trigger immediate large-scale collapse. This suggests that the gel can initially support these local macroscopic restructuring. They used a dark imaging technique to view these two features. They explained the channel formation in their system due to the flow-induced rearrangement of the particle network. The interconnected porous media of the gel may form these microchannels. The solvent may flow in these microchannels choosing the path of least resistance to reach the suspension surface. This flow might erode some gel particles that are on the channel surface, thus widening the microchannels. The increasing rapid flow of the solvent might break off material from the channel wall making the channel even wider. They observed the macroscopic channels carry fragments of broken gel to the surface of the gel. This will create regions of non-uniform concentration at the top of the gel. Dark field images show at these non-uniform concentrations the steamers first form. And that gel structure starts to break from the top. They provide no evidence, but they think the channels move some fragmented particles to the surface of the gel, creating more compact material at the top. This more compact and more concentrated material may sink in the surrounding gel causing local breaking and flow of particle network. Streamers are responsible for the macroscopic collapse of the gel. The gel network can tolerate such macroscopic disturbances in this structure for only a finite period.

It is interesting that the creeping sedimentation, which occurs at high polymer concentration, shows none of the channeling nor the streamer features. Gels that undergo

creeping sedimentation do not lose their structural integrity in a dramatic way as those shown in delayed sedimentation. Instead, these samples compress almost uniformly under their own weight.

2 Experimental Setting

2.1 Mixing and Sample Preparation

We used Carboxyl modified latex (CML) nanoparticles with a radius a = 20 nm and density of 1.05g/cm^3. To destabilize the particles, we used $MgCl_2$. A double syringe was used for mixing the samples and transferring them to plastic cuvettes with internal dimensions 1cm×1cm. The double syringe technique enables us to minimize the bubble formation by pulling the exact volume of prepared solutions without pulling air. Figure 2.1 shows the double syringe system. Data was collected at different times after the onset of aggregation. We call this time a waiting time, t_w.

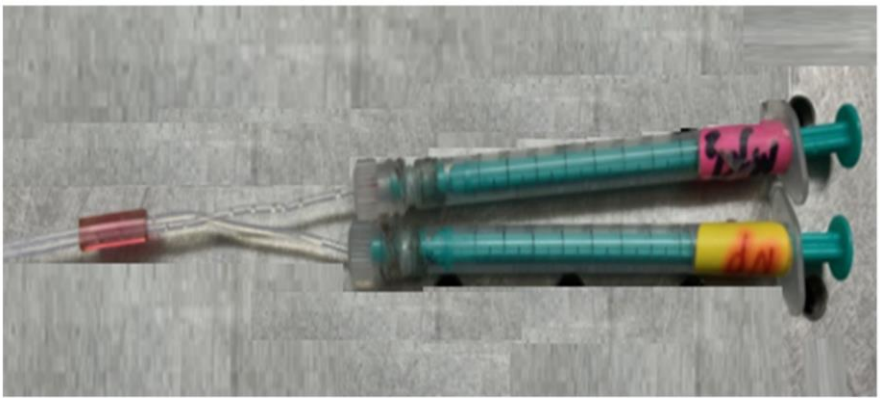

Figure 2.1. Double syringe system.

2.2 The Stability Ratio W

In Chapter 1, we discussed the two limiting regimes of aggregation: DLCA and RLCA. Fractal dimension is usually used to distinguish between these two limiting regimes. Another way to distinguish between these regimes is using and concept of W. W can be described as the inverse of sticking probability for two colliding particles. Holthoff et al. described an experimental procedure to find W (Holthoff et al., 1996). Ebini et al. modified the Holthoff method to find W that suits our gel samples (Ebini, 2020). Figure **2.2** shows the measured W vs. the salt concentration, [$MgCl_2$], for different f_{vm} values. To be able to use Figure **2.2** and apply it to my work, I choose to use the same particles size and same salt type as the ones used in the figure below.

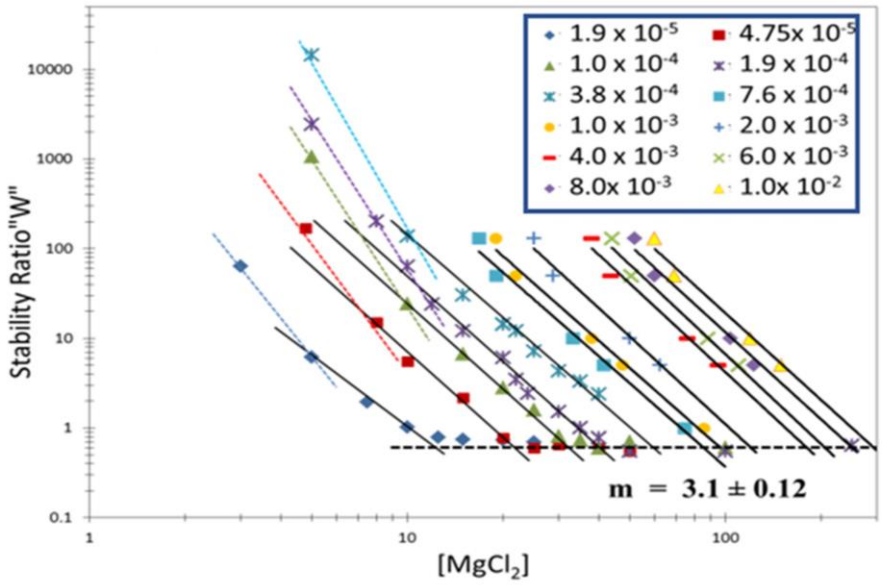

Figure 2.2. Stability Ratio, W vs. the salt concentration, [$MgCl_2$], for 20nm radius Polystyrene colloids with different f_{vm} (Ebini, 2020).

An interesting fact about W is that different systems with the same W, regardless of f_{vm} and [$MgCl_2$], will yield the same D_f. In other words, keeping the interaction potential between the monomers the same will yield the same D_f (Ebini, 2020). This is shown in Figure 2.3 where D_f vs. W is graphed for different f_{vm}.

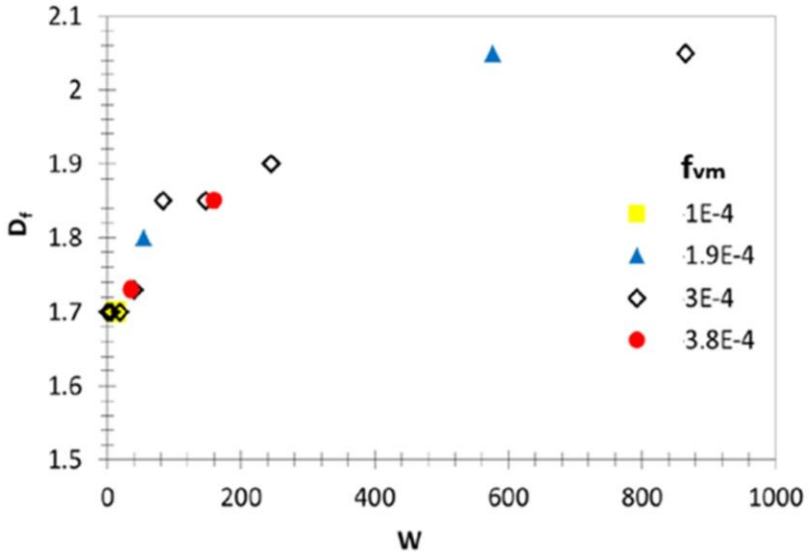

Figure 2.3. Fractal dimension D_f vs. Stability Ratio W for different f_{vm} (Ebini, 2020).

2.3 Dynamic Light Scattering (DLS) Set Up and Calibration

Dynamic Light Scattering, DLS, is a technique widely used to determine the size of colloidal particles. DLS measures the intensity fluctuation due to the motion of the particles. When colloids are suspended in a solvent, they will undergo Brownian motion. Brownian motion is a random motion of the particles that results from their collision with solvent molecules. The speed at which particles diffuse as a result of Brownian motion is proportional to the particle size. Smaller particles move or diffuse quickly, and larger particles diffuse more slowly. Hence

the intensity fluctuation depends on the particle size. DLS technique uses these intensity fluctuations and produces a function known as the intensity autocorrelation function, g_2 (t), from which we can infer the particle size if the medium viscosity is known.

Figure 2.4 shows a schematic sketch of the small and large particles' intensity fluctuations and the corresponding g_2 (t) function.

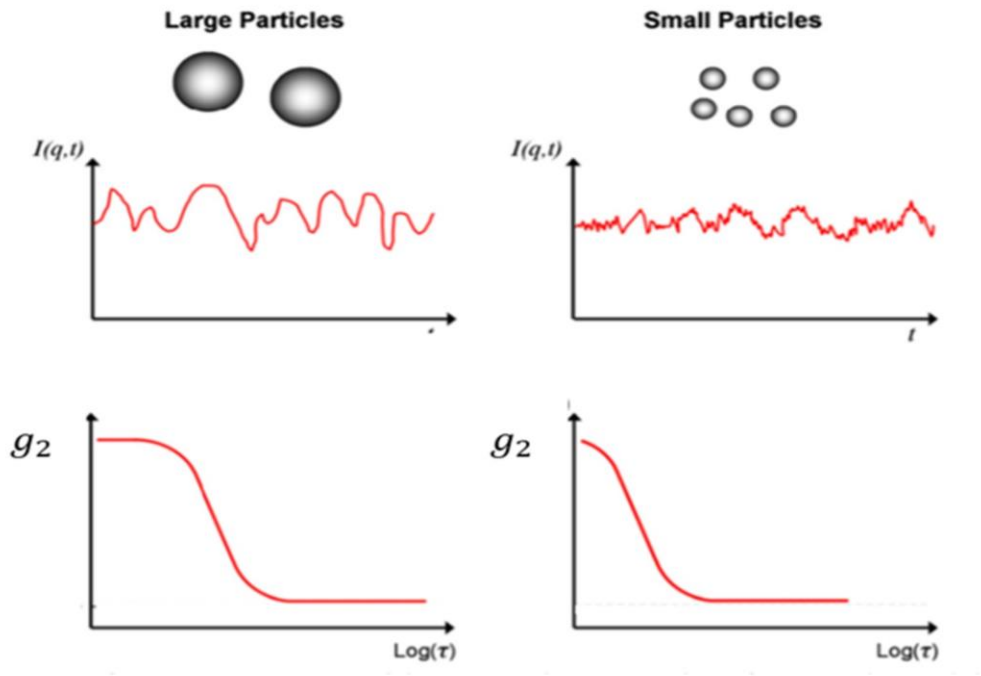

Figure 2.4. Differences between large and small particles in their intensity trace and correlation function. The scattered light fluctuates faster in smaller particles, and the correlation function decays faster (Lim et al., 2013).

The Siegert relation relates the average measured intensity autocorrelation function, g_2(t), with the normalized field autocorrelation function f_1(t)

$$g_2(t) = 1 + f_c \left| f_1(t) \right|^2 \quad (2.1)$$

Where f_c is the coherence factor which, experimentally, takes a value less than one, and $f_1(t) = C\, e^{-t/\tau}$ the decay rate of the auto correlation function is directly related to the translational diffusion coefficient D.

$$\tau = \frac{1}{q^2 D} \quad (2.2)$$

Where $D = \frac{k_B T}{6\pi\eta a}$, a is the radius of the particle, η viscosity of the medium, k_B is the Boltzmann constant, T is the temperature in Kelvin, and $q=(4\pi n/\lambda)\sin(\theta/2)$. Where λ is the wavelength, and θ is the scattering angle.

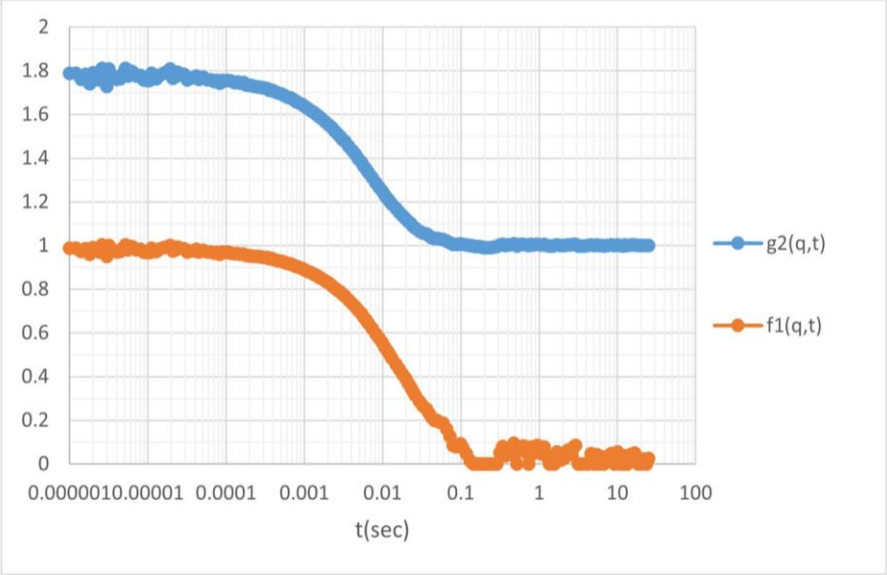

Figure 2.5. The Intensity autocorrelation function g_2(q,t), and the corresponding dynamic structure factor f_1(q,t) .

Figure 2.5 shows the $f_1(q,t)$ vs. t. The radius of the particle can be found by using $f_1(q,t)$ to determine the decay time τ. Figure 2.6 shows an example of the temporal evolution of the $f_1(t)$ function with different waiting times t_w. The sample in this figure consists of $f_{vm}= 3.8 \times 10^{-4}$, and a salt concentration of 18mM. This f_{vm} and salt concentration yields a W = 20.

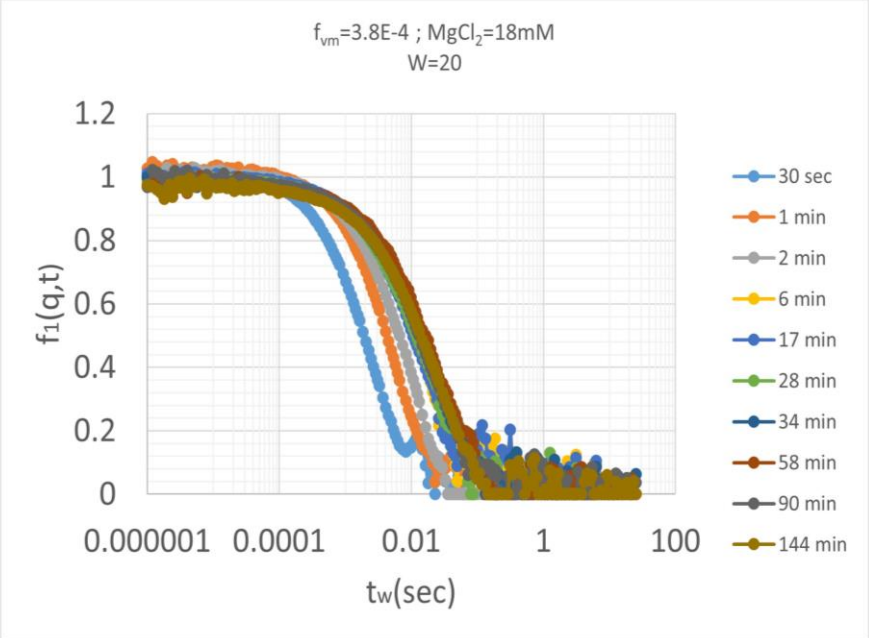

Figure 2.6. The dynamic structure factor $f_1(q,t)$ vs. t for the gelling sample of $f_{vm} = 3.8 \times 10^{-4}$, $MgCl_2$=18mM, and W = 20.

For fractal aggregates, the size measurement from DLS does not always represent the true hydrodynamic radius, R_h (Lindsay et al., 1988). We will call the radius we obtain from $f_1(t)$ vs. t graph the apparent radius, R_{app}. Lindsay et al. showed that when qR_h >>1 the rotational diffusion affects the DLS size measurement. The R_{app} tends to be smaller than R_h by a factor of 2.25. Another correction is made by Sandkuhler et al.(Sefcik et al., 2005) for qR_h >> 10 . This correction initiates from the internal dynamics of the aggregates. In our work, we get our true R_h by following both Lindsay and Sandkuhler's method.

2.4 Gel Collapse Experiment Set Up

Various compositions of samples depending on W were prepared using Figure 2.2. We experimented with a combination of monomer volume fractions and salt concentrations, hence different W values, that gelled first and then settled. We found that $f_{vm}= 3.8 \times 10^{-4}$ with W values range from 1 to 50 will satisfy our study. We sealed the samples to delay evaporation. We noticed that evaporation starts to be visible around $t_w = 14^{th}$ day of preparing the sample.

The samples were placed on an optical table to absorb any vibrations. We monitored the temporal evolution of the gel height within our experimental time that lasted between 7-10 days. The experiment was done in a room temperature. As the gel collapse, a curved interface between the colloid gel and the suspending fluid can be observed. The initial height was fixed to be equal for all the samples at $H_o = 0.75$". The evolution of the gel height was measured from the bottom to the curved interface, as shown in Figure 2.8.

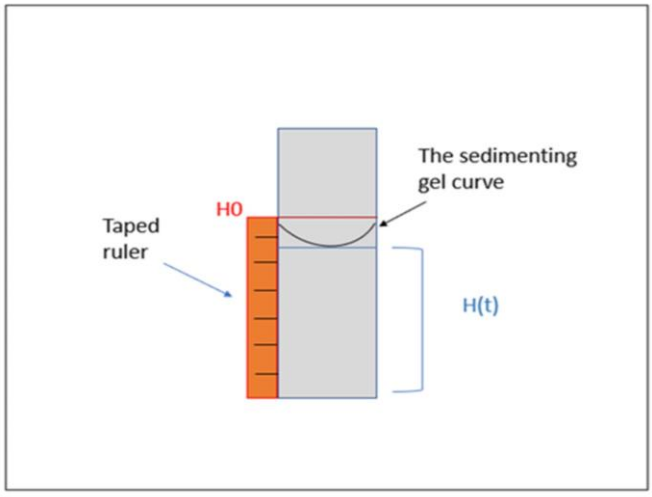

Figure 2.7. A sketch of the sample cell showing the initial height, H_o, and the settling sample height profile H(t) measured from the bottom to the curved interface.

3 Results and Discussion

The aim of this work is to study gel collapse. Hence, we need to find the proper combination of f_{vm} and [$MgCl_2$] that will gel first and then, possibly, collapse. Sorensen et al. (Sorensen & Chakrabarti, 2011) presented the IGP theory where we can predict the size of the aggregates at the gel point. Ebini et al. verified this theory experimentally on colloidal particles. They found for systems that gel, the kinetics slows down drastically at the IGP. This was evident by plotting R_h vs. t_w for different samples. The size of the aggregate at the region where the kinetics slows down was in very good agreement with the predicted $R_{g,G}$ from the IGP theory(Ebini & Sorensen, 2019), see Eq.(1.5).

We measured the size of the aggregates using DLS. This measurement yields R_h value. The IGP theory uses the radius of gyration R_g, and finds the radius of gyration at the gel point, $R_{g,G}$. Note here we consider R_h and R_g are equal, which is a good approximation given that $R_h = 0.77R_g$ (Sorensen, 2011). To calculate $R_{g,G,}$ we need the D_f value for the different samples with known W values. To find D_f we used Figure 2.3, and then we were able to calculate $R_{g,G}$ using Eq (1.5). If we find the calculated $R_{g,G}$ is approximately equal to the experimental R_h at the rounding off,and then the system gelled first then settled. If R_h at rounding off is less than $R_{g,G}$,then the system settled before it had the chance to gel.

We found the minimum f_{vm} that our system needed to possibly form a gel and then sediment to be 3.8×10^{-4}. We will name this f_{vm} as f_{vm}^{g}. For each combination of f_{vm}^{g} and [$MgCl_2$] we find the corresponding W using figure 2.3.

Figure 3.1 shows R_h vs. t_w for samples made of $f_{vm}^{g} = 3.8 \times 10^{-4}$ with different W. The figure shows R_h is starting to round off at size ≈ 4.4μm for W = 1, 5, 10, 20, and 50 and R_h ≈

0.7μm for W=100. To compare these experimental sizes at rounding off with the predicted values using Eq.(1.5), we need to know the D_f of each system. Knowing the W value is very useful here and allows us to find D_f following figure 2.3. Table 3.1 summarizes all the data graphed in figure 3.1 and shows the obtained D_f, experimental R_h, and calculated $R_{g,G}$ values.

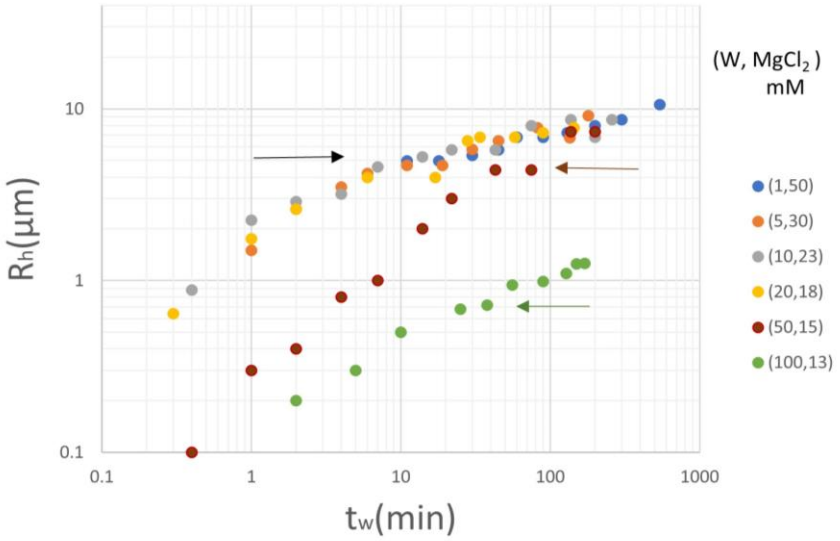

Figure 3.1. Temporal evolution of R_h for gel samples with $f_{vm} = 3.8 \times 10^{-4}$ and different salt concentrations, yielded different W. The arrows indicate R_h at rounding off.

W	$MgCl_2$ (mM)	D_f	R_h (μm) at rounding off	$R_{g,G}$(μm)
1	50	1.7 ± 0.05	4.4 ± 1.7	4.4 ± 1.01
5	30	1.7 ± 0.05	4.4 ± 1.2	4.4 ± 1.01
10	23	1.7 ± 0.05	4.4 ± 1.7	4.4 ± 1.01
20	18	1.7 ± 0.05	4.4 ± 2	4.4 ± 1.01
50	15	1.77 ± 0.05	4.4 ± 1.2	6.1 ± 2
100	13	1.85 ± 0.05	$0.7 \pm .2$	9.4 ± 1.6

Table 3.1. Summary of data in figure 3.1 with the corresponding W values, D_f values, experimental R_h, and calculated $R_{g,G}$ for $f_{vm} = 3.8 \times 10^{-4}$.

Table 3.1 shows that for $f_{vm}^g = 3.8 \times 10^{-4}$ and W = 1, 5, 10, and 20, the system indeed gelled because of the calculated $R_{g,G}$ = the experimental R_h at rounding off. Whereas for W = 50, the system is not clear if it gelled or not, but surely it is at the edge of gelling as the calculated $R_{g,G}$ is slightly bigger than the experimental R_h at rounding off. In contrast, at W=100, the system did not have the chance to gel at all.

In our exploration for a system that will gel first and then might sediment, we found four regimes of sedimentation. The first one is a cluster deposition when $f_{vm} < f_{vm}^g$. The second one is when $f_{vm} > f_{vm}^g$ where the system gelled and did not sediment, at least during our experimental time. The third one is at $f_{vm} \geq f_{vm}^g$ where the system will gel first and then sediment. Finally, at $f_{vm} \geq f_{vm}^g$, W is high enough that the system will sediment before it has the chance to gel. A schematic diagram showing these regimes is shown in figure 3.2.

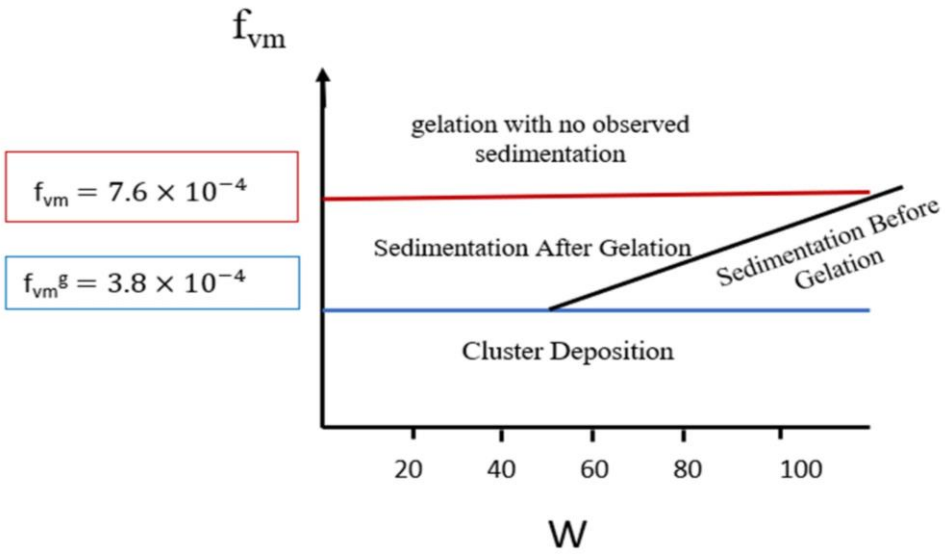

Figure 3.2. A schematic diagram represents the four different regimes we encounter in our work.

The first regime represents a system that formed aggregates, evident by the cloudy color of the sample after mixing, but far from being gelled. After a while, the aggregates start to look lumpy, and the aggregates start to fall and collect at the bottom of the cuvette. This is known as cluster deposition (Allain et al., 1995). Figure 3.3 show an example of cluster deposition f_{vm}= 1.9×10^{-4}, [$MgCl_2$] = 18 mM and W = 10.

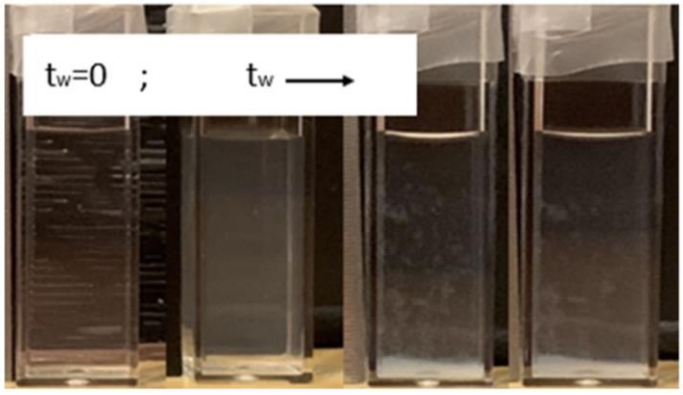

Figure 3.3. A time sequence of images for a cluster deposition.

The second regime is for gelled samples with $f_{vm} = 7.6 \times 10^{-4} > f_{vm}^{g}$, and W values range from 1 to 100. The system gelled quickly, but no sedimentation was observed within our seven days of observation. This is shown in Figure 3.4. Note that we monitor the sample exceeding the 7 days; we saw no sedimentation. On the other hand, evaporation sometimes took place before the 14th day.

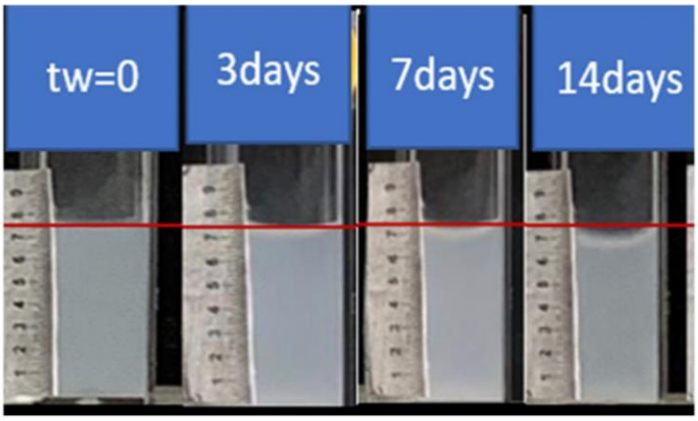

Figure 3.4. A time sequence of images for a gel sample of $f_{vm} = 7.6 \times 10^{-4}$ and W= 100. No sedimentation observed, instead evaporation starts to take place between t_w = 7-14 days.

The third regime occurred at $f_{vm} = f_{vm}^{g} = 3.8 \times 10^{-4}$ with $1 \leq W < 50$. In this regime, the sample gelled first, and after some delay time, it settled. This is the regime that we want to investigate further. We monitor the temporal height profile for these samples for seven days. Figure 3.5 shows an example of H(t) vs. t_w for W=50. From this graph, we determine the sedimentation time t_s, which is the time when sedimentation was first observed.

The fourth regime is when the samples sediment before they gel. This is different than cluster deposition. In this regime, the $f_{vm} \geq f_{vm}^{g}$ with high enough W. An example of this regime is $f_{vm} = 3.8 \times 10^{-4}$ and W = 100. Our DLS measurement for R_h showed that the system did

sediment before it gel, but the sample did not collapse completely to the bottom of the cell like the cluster deposition. Instead, it collapses to a stable finite height that could hold its own weight.

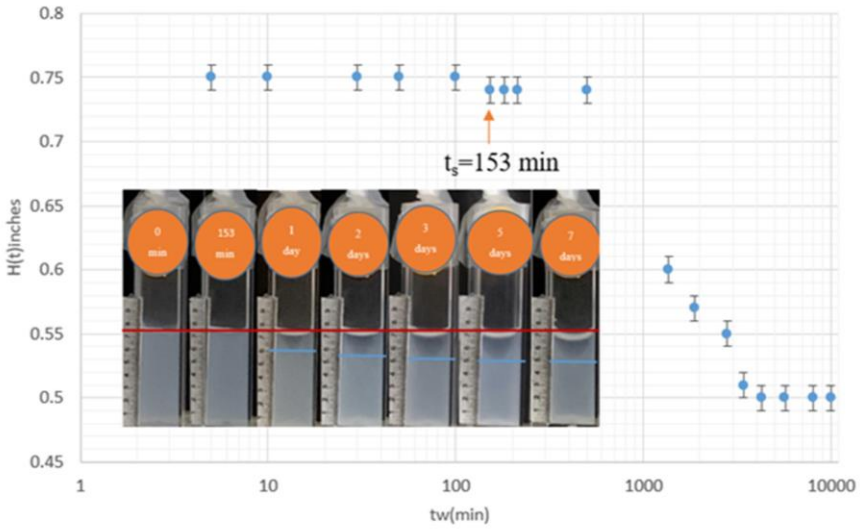

Figure 3.5. The evolution of the height for gel sample of $f_{vm} = 3.8 \times 10^{-4}$ and W=50 versus the waiting time t_w. The insert is a time sequence of images for this sample.

Figure 3.6 shows H(t) vs. t_w for all the samples summarized in Table 1. We obtain t_s from this figure. This figure shows for a collapsed gel, the higher W, the faster gel collapse kinetics. In addition, the asymptotic height, H_a, has a higher value with smaller W. Note that W =100 does not follow this pattern because the sample sediment away before it gelled. And remember that W=50 we suspect that the gelation and sedimentation times were comparable. From figure 3.6 we obtained the t_s and H_a and graphed them as a function of W as shown in figure 3.7 (a) and (b) respectively. These graphs shows that both t_s and H_a are a decreasing function of W.

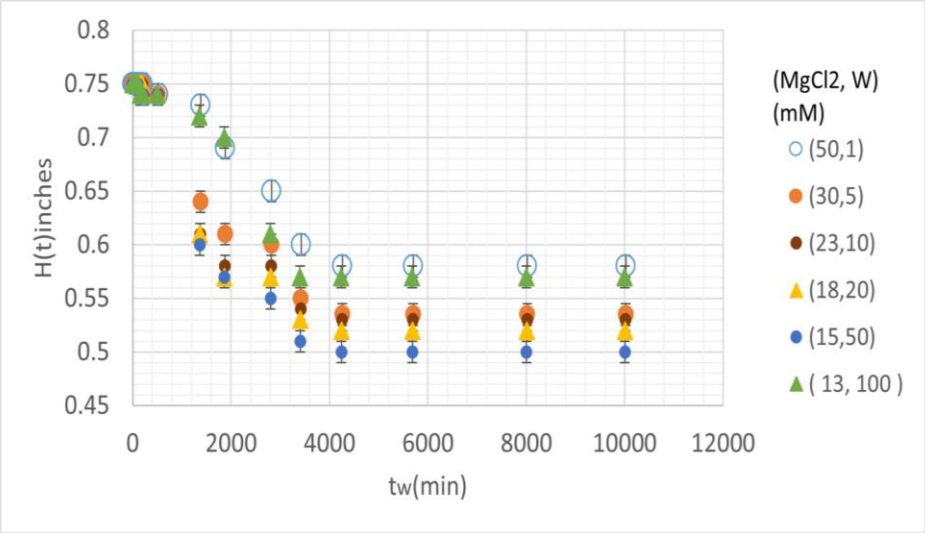

Figure 3.6. The evolution of the sedimenting gel height vs. the waiting time, t_w for $f_{vm} = 3.8 \times 10^{-4}$ with different [$MgCl_2$] and W values.

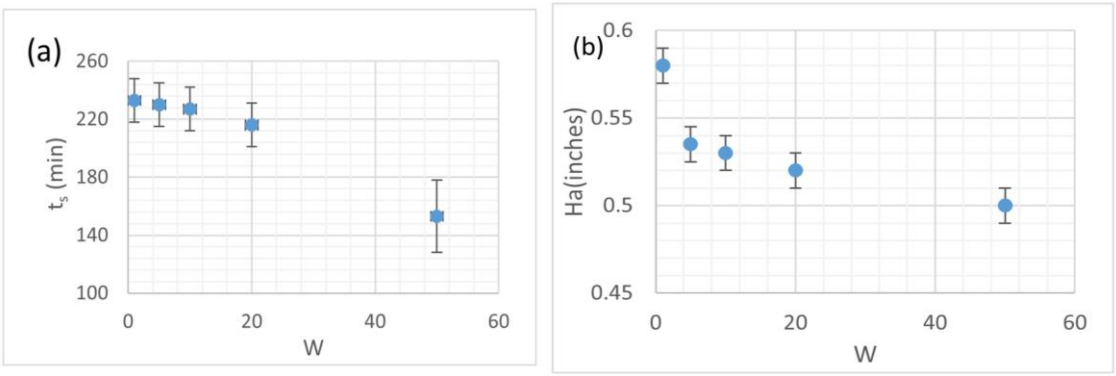

Figure 3.7. (a) Sedimentation time, t_s, vs. W, (b) asymptotic height, Ha, vs. W for $f_{vm} = 3.8 \times 10^{-4}$.

To study gel collapse kinetics, we plot H(t) vs. t_s as shown in Figure 3.8(b). This graph shows the gel collapse kinetics is slower for smaller W. From this graph we find the characteristic decay time, t_c. Figure 3.8(b) shows t_c vs. W. This indicates t_c is decreasing with increasing W.

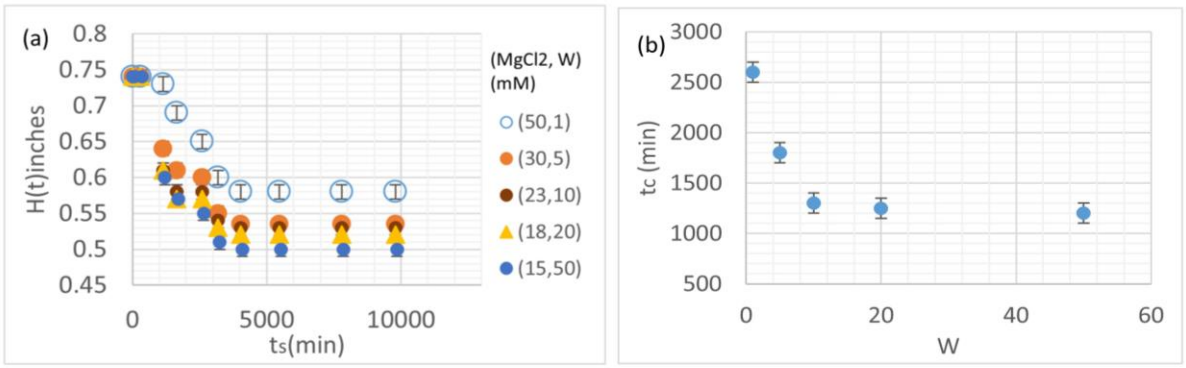

Figure 3.8. (a) H(t) vs. the sedimenting time, t_s, (b) t_c vs. W for $f_{vm} = 3.8 \times 10^{-4}$.

Our results can be summarized by the following: with decreasing W, t_s and H_a are increasing while t_c is decreasing. In other words, with decreasing W, the gel withstands its own weight for longer times in comparison to higher W values. Eventually, the gel will face a collapse and start compacting up to the point it reaches a finite final height. The collapse kinetics is slower with small W, and the gel seems to have a higher ability to resist the compaction. Recall W indicates the strength of the interaction between particles. The smaller the W the stronger the attraction forces compared to the repulsive forces in the DLVO potential. In other words, the sticking probability between monomers is biggest for smallest W. This means smaller W values create stronger gels. In addition, smallest W results in smallest D_f value. Remember smaller D_f means less dense fractal aggregates. Hence, for a gel with the same f_{vm}, the smaller W yields not just smaller $R_{g,G}$ but also lighter aggregates. This will yield less gravitational stresses on the gel to bare its own weight for longer times. And even when it faces the collapse, it compacts the least. Additionally, the gel collapse kinetic is slow at small W. This might provide the collapsed gel longer time to restructure and probably form a new gel at H_a with this new f_{vm} at the final height. More work needs to be done to test these to ideas.

Harich et al. and Starrs et al. observed two different behaviors for colloidal gels destabilized using depletion interaction. The first one is the delayed sedimentation characterized by a delay time followed by a linear rapid collapse which followed by a stretched exponential. The second one is creeping sedimentation or stretched exponential sedimentation two different behaviors for colloidal gels destabilized using depletion interaction. To distinguish what type of sedimentation our data represent, we followed Harich et al. and plot $(H(t)-H_a)/(H_0-H_a)$ vs. t_w as shown in figure 3.9. The decay of the gel height consists of a linear collapse followed by an exponential. This indicates the sedimentation in this $f_{vm,}$ and W range might be classified as a rapid sedimentation.

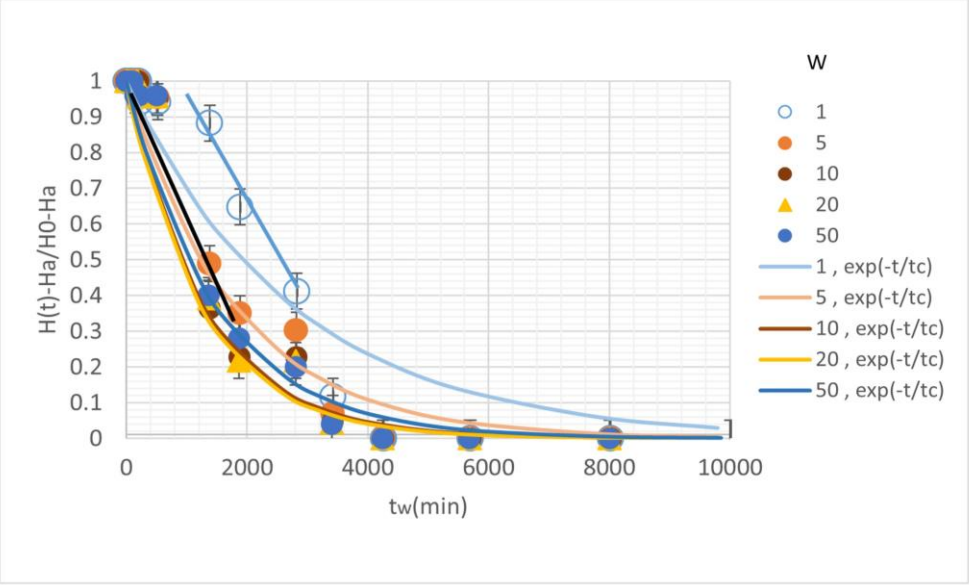

Figure 3.9. $((H(t)-H_a)/(H_0-H_a))$ vs. t_w for $f_{vm} = 3.8 \times 10^{-4}$ .The fit is linear collapse followed by an exponential function.

4 Conclusion

In this work we investigated the effect of stability ratio, W, on the sedimentation of colloidal gels. We monitored the temporal evolution of the gel height within our experimental time that lasted about 7 days. We used polystyrene spheres with radius 20nm and density of 1.05g/cm3. For these particles we found the f_{vm} for the system to gel is $f_{vm}^{g} = 3.8 \times 10^{-4}$. If $f_{vm} < f_{vm}^{g}$ cluster deposition was observed and the clusters fall down to the bottom of the cell. If $f_{vm} > f_{vm}^{g}$, the system will gel. For the gelled samples, the system either sediment after some delayed time or never settle depending on the value of the interaction, quantified experimentally by W. In addition, there is a regime where $f_{vm} \geq f_{vm}^{g}$ but W is high enough that the system will sediment before it has the chance to gel. For settling gels, the sedimentation height reached an asymptotic value, H_a. In addition, we found that the temporal evolution of the sedimentation height profile depends on W in two manners. First, the characteristic time of the sedimentation height, t_c, increases with decreasing W. In other words, the sedimentation has faster kinetics for higher W. Second, we found that H_a decreases with increasing W. We provided a physical picture to explain these two observations.

In future work I suggest testing these speculations by changing the f_{vm} for settling gels. In addition, some work shows that for creeping sedimentation, the size of the cuvette matter (Starrs et al., 2002). While others like Manley et al think it is not a function of height (Manley et al., 2005). It will be interesting to test that by changing the initial height and / or the cuvette size.

5 References

Allain, C., Cloitre, M., & Wafra, M. (1995). Aggregation and sedimentation in colloidal suspensions. *Physical Review Letters*, *74*(8), 1478–1481. https://doi.org/10.1103/PhysRevLett.74.1478

Condre, J. M., Ligoure, C., & Cipelletti, L. (2007). The role of solid friction in the sedimentation of strongly attractive colloidal gels. *Journal of Statistical Mechanics: Theory and Experiment*, *2*. https://doi.org/10.1088/1742-5468/2007/02/P02010

Ebini, R. H. (2020). *A light scattering study of the kinetics of the sol-to-gel transition in particulate systems*.Kansas State University.

Ebini, R. H., & Sorensen, C. M. (2019). Light scattering studies of the sol-to-gel transition in particulate systems. *Journal of Colloid and Interface Science*, *556*, 577–583. https://doi.org/10.1016/j.jcis.2019.08.075

Harich, R., Blythe, T. W., Hermes, M., Zaccarelli, E., Sederman, A. J., Gladden, L. F., & Poon, W. C. K. (2016). Gravitational collapse of depletion-induced colloidal gels. *Soft Matter*, *12*(19), 4300–4308. https://doi.org/10.1039/c5sm02651b

Holthoff, H., Egelhaaf, S. U., Borkovec, M., Schurtenberger, P., & Sticher, H. (1996). Coagulation rate measurements of colloidal particles by simultaneous static and dynamic light scattering. *Langmuir*, *12*(23), 5541–5549. https://doi.org/10.1021/la960326e

Kim, J. M., Fang, J., Eberle, A. P. R., Castañeda-Priego, R., & Wagner, N. J. (2013). Gel transition in adhesive hard-sphere colloidal dispersions: The role of gravitational effects. *Physical Review Letters*, *110*(20), 1–5. https://doi.org/10.1103/PhysRevLett.110.208302

Lim, J., Yeap, S. P., Che, H. X., & Low, S. C. (2013). Characterization of magnetic nanoparticle by dynamic light scattering. *Nanoscale Research Letters*, *8*(1), 1–14. https://doi.org/10.1186/1556-276X-8-381

Lindsay, H. M., Klein, R., Weitz, D. A., Lin, M. Y., & Meakin, P. (1988). Effect of rotational diffusion on quasielastic light scattering from fractal colloid aggregates. *Physical Review A*, *38*(5), 2614–2626. https://doi.org/10.1103/PhysRevA.38.2614

Mandelbrot, Benoit B. 1977. *Fractals: Form, Chance, and Dimension*. Vol. 706. WH Freeman San Francisco.

Manley, S., Skotheim, J. M., Mahadevan, L., & Weitz, D. A. (2005). Gravitational collapse of colloidal gels. *Physical Review Letters*, *94*(21). https://doi.org/10.1103/PhysRevLett. 94.218302.

Sefcik, J., Grass, R., Sandkühler, P., & Morbidelli, M. (2005). Kinetics of aggregation and gelation in colloidal dispersions. *Chemical Engineering Research and Design*, *83*(7 A), 926–932. https://doi.org/10.1205/cherd.05027

Sorensen, C. M. (2011). The mobility of fractal aggregates: A review. *Aerosol Science and Technology*, *45*(7), 765–779. https://doi.org/10.1080/02786826.2011.560909

Sorensen, C. M., & Chakrabarti, A. (2011). The sol to gel transition in irreversible particulate systems. *Soft Matter*, *7*(6), 2284–2296. https://doi.org/10.1039/c0sm00228c

Starrs, L., Poon, W. C. K., Hibberd, D. J., & Robins, M. M. (2002). Collapse of transient gels in colloid-polymer mixtures. *Journal of Physics Condensed Matter*, *14*(10), 2485–2505. https://doi.org/10.1088/0953-8984/14/10/302